Impact of feed mixture control on arc behaviour in direct-current arc furnace smelting of chromite – a modelling study

by Q.G. Reynolds,[1,2], M.W. Erwee[3], S. Swanepoel[3], R. Fourie[3]

Affiliation:
1 Pyrometallurgy Division, Mintek, Johannesburg, South Africa
2 Stellenbosch University, Stellenbosch, South Africa
3 Samancor Chrome Ltd, Johannesburg, South Africa

Correspondence to:
Q.G. Reynolds

Email:
quinnr@mintek.co.za

Dates:
Received: 19 May. 2026
Published: July 2026

How to cite:
Reynolds, Q.G., Erwee, M.W., Swanepoel, S., Fourie, R. 2026. Impact of feed mixture control on arc behaviour in direct-current arc furnace smelting of chromite – a modelling study. *Journal of the Southern African Institute of Mining and Metallurgy*, vol. 126, no. 7, pp. 427 – 434

DOI ID:
https://doi.org/10.17159/2411-9717/1105/2026

ORCiD:
Q.G. Reynolds
https://orcid.org/0000-0002-5196-8586
M.W. Erwee
https://orcid.org/0000-0001-5067-3439
S. Swanepoel
https://orcid.org/0000-0001-5067-3439
R. Fourie
https://orcid.org/0009-0008-3503-0513

This paper is based on a presentation given at the SAIMM Pyrometallurgy International Conference 2026, 26-28 May 2026, CSIR International Convention Centre, Pretoria, South Africa

Abstract

Unexpected excursions in electrode hoist position are occasionally observed on direct-current arc furnace plants producing ferrochromium, and are not readily explained by changes in electrical power supply or known process disturbances. One possible mechanism for this is variations in feed reductant balance altering the freeboard gas composition and, hence, the thermophysical properties of the arc plasma, changing the arc's effective electrical resistance. This hypothesis is investigated using an integrated computational modelling workflow comprising thermochemical equilibrium simulations in FactSage, plasma property calculations using the open-source minplascalc tool, and magnetohydrodynamic arc simulations using the open-source plasmaArc solver. Three reductant balance conditions were examined across a range of effective slag temperatures. Results show that while the reductant balance does influence freeboard gas composition and certain plasma properties (particularly electrical conductivity and radiation emission coefficient when lower slag temperatures are considered), these two effects act in opposing directions and largely cancel one another. Arc voltages and resistances are consequently not significantly different between reductant conditions. It is concluded that variations in feed reductant balance are unlikely to be the primary cause of the observed hoist excursion events via this mechanism, and directions for future investigation are proposed.

Keywords

pyrometallurgy, ferrochromium, plasma, modelling.

Introduction

Chromium is a critical mineral in South Africa, which harbours most of the world's known ore reserves. It is used primarily as an alloying agent in the manufacture of stainless steel and other specialised metal products. The majority of the chromium supply worldwide is produced as a ferrochromium (FeCr) alloy by carbothermic reductive smelting of chromite ore in electric furnaces (Gasik, 2013; Jones, 2014).

Contemporary pyrometallurgical processes for FeCr production use blended carbonaceous reductants, typically fossil metallurgical coke, coal, and/or anthracite, as a reducing agent and produce significant scope-1 CO_2 emissions. Reducing the carbon footprint of the alloy product is desirable, and several new concepts for low-carbon FeCr production are under investigation. These include the use of plasma-state hydrogen (Dalaker, Hovig, 2023) or light metals (Akhmetov et al., 2025) as replacements for carbonaceous reductants. Many of these concepts are however still at early stages of development, and it is argued by some that carbonaceous reductants from biological sources can be used to achieve carbon-neutral smelting more rapidly and without radical changes to existing furnace designs or process chemistry (Sommerfeld et al., 2024). It is therefore likely that carbothermic smelting in some form will continue to be used for FeCr production in the post-decarbonisation landscape, and studies of such processes remain relevant.

Open arc, open bath direct-current (DC) plasma arc furnace technology is particularly well-suited to chromite smelting due to its ability to handle fine feed materials and high temperatures (Jones, 2014; Oterdoom et al., 2025; Sager et al., 2010). DC furnaces consist of a closed cylindrical crucible, which contains the process material, and one or more graphite electrodes entering through the vessel roof. An electric arc is formed between the electrode tip and the surface of the molten bath below it. The plasma arc is a sustained electrical discharge, which transfers thermal and mechanical energy to the molten bath, which in turn drives the thermochemistry of the reduction process (Boulos et al., 2023; Bowman, Krüger, 2009). Chromite ore and carbonaceous reductants such as metallurgical coke are fed to the furnace together with fluxes and chemical modifiers, producing a waste slag and the FeCr-product alloy.

Impact of feed mixture control on arc behaviour in direct-current arc furnace smelting

For optimal metallurgical performance, electrical control of DC furnaces is important to ensure that open arc operation and correct power input to the process are maintained at all times (Geldenhuys, 2017). This is generally accomplished by a series of nested control loops, the outermost of which moves the electrode hoist up or down to meet a desired furnace voltage or resistance setpoint (Sager et al., 2010). Even with such control measures, large variations in hoist position are sometimes observed on furnace plants and would seem to indicate sudden changes in the effective resistance of the furnace.

An example of this can be seen in data obtained from an industrial FeCr DC furnace plant shown in Figure 1. The period displayed is the time between electrode section additions and covers approximately 10 taps. It can be seen that although the furnace current and voltage are being controlled close to their setpoints, there is a considerable degree of variation in the hoist position, which is a proxy for the arc length inside the furnace. The nett downward trend through the period is expected due to electrode erosion, which occurs at a constant rate at fixed power and current (Kjellberg, Stenkvist, 1989), but the intermittent movements of the hoist up or down (some examples are highlighted with the red arrows) can be rapid and significant. These excursions are not accounted for by changes in the electrical power supply, nor do they appear to correlate with known process disturbances such as furnace tapping or feed interruptions.

Possible explanations for such behaviour are slag foaming events, collapse of feed banks, electrode damage or breakage, sudden changes in process chemistry, power/feed imbalances, and others. The mechanisms by which these could affect the furnace resistance include altering the chemical composition or temperature of the slag bath, changing the geometry of the bath or electrode, or changing the gas composition in the freeboard space (and hence, the electrical properties of the arc plasma).

In this paper, the authors apply an integrated arc modelling workflow comprising thermochemistry simulations, plasma property calculations, and computational multiphysics models of the plasma arc to study process chemistry variations and their effect on freeboard gas composition as a possible explanation for these events. The impact of over- or under-feeding reductant for a given FeCr feed mixture is examined for the case of a representative industrial-scale DC furnace, and the results are discussed in terms of their effect on the electrical behaviour of the arc.

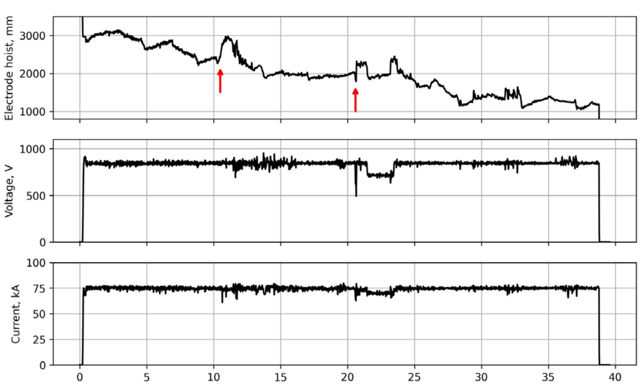

Figure 1—Hoist position and electrical measurements from a DC furnace producing FeCr (red arrows indicate start of hoist excursion events)

Description of modelling workflow

The plasma arc in a DC arc furnace is a high-velocity (km/s), high-temperature (10,000 K) jet sustained by electromagnetic forces acting on thermally ionised gas in the freeboard space above the molten bath. Its ability to conduct electrical current and transfer large quantities of mechanical and thermal energy to the bath makes it the primary energy delivery mechanism of the furnace, and understanding its behaviour is central to the effective operation of DC arc furnace processes (Bowman, Krüger, 2009; Geldenhuys, 2017).

The extreme operating conditions of large-scale metallurgical arcs limit direct experimental characterisation in most cases. Computational modelling provides a practical alternative, and modern approaches have advanced to the point where integrated workflows can account for the effect of metallurgical chemistry on plasma gas composition, and consequently on the thermophysical properties of the plasma (Reynolds et al., 2025a). The modelling workflow employed in the present study consists of three separate steps:

- ➤ The first step in the workflow uses the FactSage thermochemical simulation tool (Bale et al., 2016) to compute multiphase thermodynamic equilibria for the process under consideration. Equilibrium calculations were performed using appropriate alloy, oxide, and ideal-mixture gas databases, with feed material composition and process temperature as inputs, yielding the species composition of the gas phase.
- ➤ The freeboard gas compositions were then passed to minplascalc (Reynolds et al., 2025b), an open-source plasma property calculator, which determines equilibrium plasma compositions via Gibbs free energy minimisation and computes thermodynamic (density, enthalpy, heat capacity) and transport (viscosity, electrical conductivity, thermal conductivity, radiation emission coefficient) properties as functions of temperature at atmospheric pressure. The resulting property data are stored in lookup-table format for use in subsequent calculations.
- ➤ Finally, the plasma property data is used in plasmaArc (Reynolds, 2026), an open-source computational multiphysics solver implemented within the OpenFOAM® framework (OpenCFD Ltd, 2025) to compute the spatial and temporal evolution of the arc. The solver uses a finite-volume formulation on unstructured meshes to calculate numerical solutions to the coupled magnetohydrodynamic (MHD) governing equations describing fluid flow (Equation 1), energy transport (Equation 2), and the electromagnetic field (Equation 3):

$$\frac{\partial}{\partial t}(\rho\mathbf{u}) + \nabla\cdot(\rho\mathbf{u}\otimes\mathbf{u}) + \nabla P = \nabla\cdot\boldsymbol{\tau}_{\mathrm{ij}} + \mathbf{j}\times \qquad [1]$$
$$\frac{\partial\rho}{\partial t} + \nabla\cdot(\rho\mathbf{u}) = 0$$

$$\frac{\partial}{\partial t}(\rho h) + \nabla\cdot(\rho\mathbf{u}h) = \nabla\cdot(\kappa\nabla T) + \nabla\cdot\left(\frac{5k_BT}{2e}\mathbf{j}\right) + \frac{\mathbf{j}\cdot\mathbf{j}}{\sigma} + Q_m - Q_R$$
$$Q_m = \nabla\cdot(\boldsymbol{\tau}_{ij}\cdot\mathbf{u}) - \frac{\partial}{\partial t}(\rho K) - \nabla\cdot(\rho\mathbf{u}K) + \frac{\partial P}{\partial t} \qquad [2]$$

$$\nabla\cdot\mathbf{j} = 0, \qquad \text{with } \mathbf{j} = -\sigma\left(\nabla\phi + \frac{\partial\mathbf{A}}{\partial t} - \mathbf{u}\times\mathbf{B}\right) \qquad [3]$$
$$\nabla^2\mathbf{A} = -\mu_0\mathbf{j}, \qquad \text{with } \mathbf{B} = \nabla\times\mathbf{A}$$

In Equations 1 to 3, ρ is the plasma density, $\mathbf{u}$ is the velocity field, P is the pressure, τ_{ij} is the viscous stress tensor, j is the current density, $\mathbf{B}$ is the magnetic flux density, h is the enthalpy, κ is the thermal conductivity, T is the temperature, σ is the electrical conductivity, $K=(½)\,|\mathbf{u}|^2$ is the specific kinetic energy, Q_r is the thermal radiation loss, ϕ is the electric potential, and $\mathbf{A}$ is the magnetic vector potential. The system of equations is solved subject to boundary conditions described by the authors in previous publications (Reynolds, 2020; Reynolds et al., 2026).

Results and discussion

Three sets of conditions were considered for the DC FeCr smelting process: one with a carbon feed fraction as per normal operations, one with 33% lower carbon feed, and one with 25% higher. The gas phase compositions for each condition were obtained from thermochemical modelling at a range of different slag bath temperatures from a representative process temperature, 1800 ºC, up to the point at which no solid or liquid phases remain, approximately 3500 ºC. Temperatures approaching the boiling point of process slags are possible in the region where the extremely hot arc plasma connects to the molten bath surface (Barcza et al., 1990), and it is likely that the freeboard gas in the region near to the arc will be partially contaminated with this “vaporised” process material. The gas compositions for each process condition and slag temperature were then used to calculate the associated plasma properties as a function of plasma temperature, and the properties were passed into the MHD arc model to simulate the resulting arc behaviour in an industrial DC FeCr furnace.

Freeboard gas compositions

Thermochemical simulations were performed in the Equilib module of FactSage 8.0. For the gaseous species, the FactPS database was used, with the "include gaseous plasma" option turned on. For oxides, slag, and alloy, the FTOxid and SGTE2017 solution databases were used, respectively. Simulations were done assuming pure SiO_2 and CaO as fluxes, and pure C as reductant. The ore composition used was for a typical LG6 concentrate from the western limb of the Bushveld Complex. The composition, in mass%, was: 15.29% Al2O3, 0.36% CaO, 42.65% Cr_2O_3, 24.78% FeO, 10.65% MgO, 0.21% MnO, 4.54% SiO_2, and 0.64% TiO_2 (Swanepoel et al., 2022). Calculations were performed across a temperature range of 1550 ºC to 3500 ºC in steps of 5 ºC, spanning from the alloy tapping temperature up through the operating temperature range of the DC furnace (nominally ~1800 ºC) and beyond. Alloy chemistry and phase equilibria were evaluated at 1550 ºC, representative of the alloy tap temperature, while slag chemistry was assessed at 1800 ºC, representative of the process temperature. This staged approach provides a consistent baseline for comparing simulation cases. It is acknowledged that industrial smelting does not proceed at full thermodynamic equilibrium; the simulated values are therefore indicative of expected trends rather than absolute predictions. The simulation for the normal case had a target CaO/SiO_2 mass ratio in the slag of 0.87, with a target Si content in the alloy of 0.2% at 1550 ºC, based on pilot plant trials of MG-chromite at Mintek (Geldenhuys, 2013). For the under- and over-carbon simulations, the reductant quantity was 33% lower and 25% higher than the normal case, respectively, and was chosen such that the alloy would fall outside of customer specification: insufficient Cr recovery in the under-carbon case, and excessive Si in the over-carbon case.

The results of the thermochemical calculations are shown in Figure 2. In all conditions the gas phase is dominated by the reaction product carbon monoxide. However, it can be seen that trace metallic elements contaminate the gas to some degree in all cases, except for the lowest slag temperatures. As a general trend the fraction of metallic contaminants increases as the slag temperature rises, as a result of the increasing vapour pressure of the oxide components. Magnesium is the most volatile of the slag components, followed by silicon (in the form of SiO gas). Iron and chromium, although not particularly volatile, are also present in significant quantities due to their high concentrations in the feed ore.

The effect of increasing the reductant fraction in the feed mix is quite marked. Magnesium and silicon evaporation begins at lower slag temperatures and reaches higher levels as the reductant fraction is increased. The opposite behaviour is observed for iron and chromium, but this is a weaker trend and may simply be a dilution effect due to the increase in the other metallic components. Of the more minor components, calcium and aluminium start to appear in significant quantities only in the over-carbon case.

Plasma properties

The elemental gas compositions obtained for each reductant condition were used as inputs to a parallelised calculation of the associated plasma thermophysical properties at a range of selected slag temperatures. The full set of plasma species considered included Al, Cr, Mg, Fe, Mn, Ca, Ti, C, and O in atomic form; Alz+, Crz+, Mgz+, Fez+, Mnz+, Caz+, Tiz+, Cz+, and Oz+ as ions (where z denotes the charge number, ranging from 1 to 3), and CO, CO_2, O2, MgO, AlO, SiO, CaO, TiO, CrO, and FeO as molecular species. Calculations were performed using minplascalc

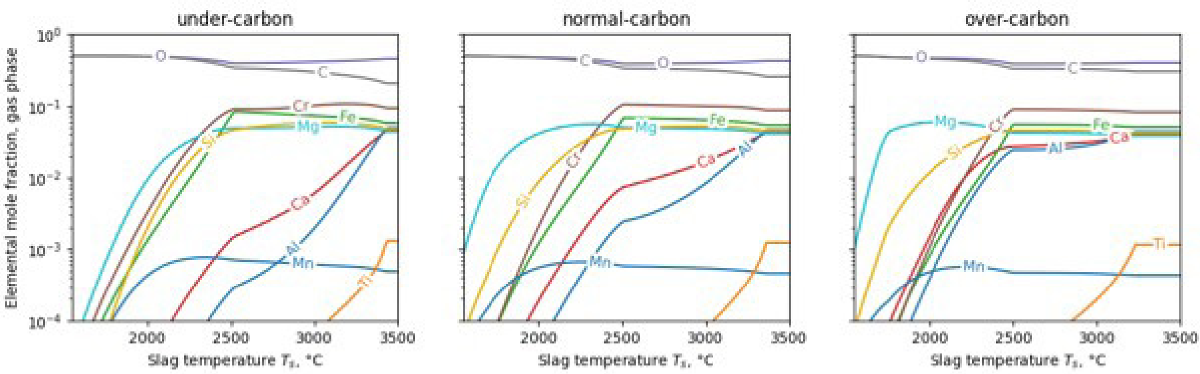

Figure 2—Elemental molar composition of gas phase in equilibrium with FeCr process alloy and slag for different reductant contents in feed

1.0.2, with the required quantum mechanical data for each species obtained from sources documented in Reynolds et al. (2025a). To improve computational efficiency, species of which the constituent elements were absent or negligible in the FactSage gas composition were excluded from the calculations. Plasma composition and thermophysical property calculations were carried out over the temperature range 300 K – 25000 K at a pressure of one atmosphere. At temperatures below 2000 K, reduced species sets were employed to avoid numerical instabilities arising from charged-particle concentrations approaching machine precision.

Plasma property results for gas compositions at slag temperatures of 1800 ºC are shown in Figure 3. At this temperature, the freeboard gas is mostly CO with small amounts of Mg and Si. The effect of changing the carbon balance is negligible for all properties, with the exception of electrical conductivity in the temperature range between 5000 K and 10000 K, and the radiation emission coefficient between 2500 K and 15000 K. For both of these properties increasing the carbon fraction in the feed results in higher values, mainly due to the increase in metallic contaminants, which ionise more easily at lower plasma temperatures.

Properties for gas compositions at slag temperatures of 3500 ºC are shown in Figure 4. At such elevated temperatures the freeboard gas is heavily contaminated with a large number of metallic species and additional oxygen from the evaporating slag. Interestingly, the overall effect of this is to move the influence of the carbon balance away from the electrical conductivity and radiation emission properties, which are almost identical, to the heat transfer properties of heat capacity and thermal conductivity. These show some differences in the low-temperature peaks, with increased carbon in the feed mixture resulting in higher peaks.

MHDmodelling

Computational multiphysics simulations of the arc in an industrial-scale DC arc furnace were set up using the properties calculated in the afore-mentioned. Separate cases were generated for each combination of slag temperature and reductant balance, with common parameters, as shown in Table 1.

A hemispherical region of the freeboard around the arc was simulated in each case. This region included the arc as well as the tip portion of the electrode and the surface of the slag bath (see Figure 5). Free inflow/outflow boundaries were applied at the surface of the hemisphere to allow mass and energy to be exchanged with the bulk furnace freeboard gas. Although the arc can create a significant depression in the molten slag bath surface at industrial scales due to the stagnation force of the jet (Bowman, Krüger, 2009), this effect was ignored in the present work for the purpose of simplification.

For each model case the calculation was conducted in two stages. In the first stage, using a low-resolution mesh, the arc was initiated in a stagnant region of plasma and simulated until representative flow patterns became established and initial conditions decayed away (typically 100 ms). In the second stage, the model was bootstrapped on the full-resolution mesh using interpolated field values from the first stage and operated for an additional 50 ms to generate data for analysis. Arc voltages were recorded at regular intervals during the simulation as the difference between the minimum and maximum of the electric potential field. The trends were then post-processed using Python scripts to obtain statistical properties of the arc voltage.

Voltages from the model cases for different reductant mixes and slag temperatures are given in Figure 6. It is immediately obvious that the slag temperature at which the freeboard gas is generated has a very strong effect on both the magnitude and behaviour of the voltages; lower temperatures produce higher arc voltages, and more chaotic and unstable operation with large variations over short time scales. In contrast, the effect of reductant balance appears to be rather negligible, especially at higher slag temperatures.

Table 1
MHD model parameters for FeCr arc simulations

Parameter	Value
Electrode diameter	0.75 m
Arc length	0.4 m
Arc current	75 kA
Cathode spot current density	1 kA/cm^2
Vaporisation temperature (cathode)	4100 K
Vaporisation temperature (anode)	3500 K
Bulk freeboard temperature	1800 K
Time simulated	50 ms
Mesh resolution (arc region)	4 mm

The differences in arc structure and dynamics are visible in Figure 7, where instantaneous temperature fields are compared between the T_s = 1800 ºC and 3500 ºC cases using the plasma properties associated with the normal-carbon balance. The effective slag temperature has a dramatic effect on the arc stability with higher values of T_s producing relatively compact, steady, and symmetrical arc jets compared to the turbulent flow patterns and highly distorted and chaotic shapes that are seen at lower values.

A statistical analysis of the voltage traces shown in Figure 6(a) for a slag temperature of 1800 ºC is shown in Figure 8. Although there are some differences, these are not particularly significant and the averages lie within one standard deviation of one another – this confirms that there is no consistent upward or downward trend in the arc voltages with carbon addition. Given that some differences were observed in both the freeboard gas compositions and the plasma properties as the reductant balance was changed, it is of interest to further investigate this.

In the next set of cases, the sensitivity of the system to the two plasma properties that showed the most differences in Figure 3, plasma electrical conductivity σ and total radiation emission coefficient ε_{tot}, was examined. This was done by holding all properties fixed and equal to the normal-carbon condition except for the property being examined, values for which were taken from the relevant over- or under-carbon plasma property dataset. This allows the effect of the individual property to be isolated.

The Effect of electrical conductivity

The effect of electrical conductivity on the arc simulation results are shown in Figure 9 and Figure 10. It is clear that less reductant in the process feed results in a higher arc voltage, at least for the under-carbon case, where the results are statistically well-separated.

It is likely that this trend is due to the increase in plasma electrical conductivity that accompanies increased reductant addition. Increasing electrical conductivity would be expected to produce a more conductive arc and, hence, a lower voltage if all other parameters are kept the same.

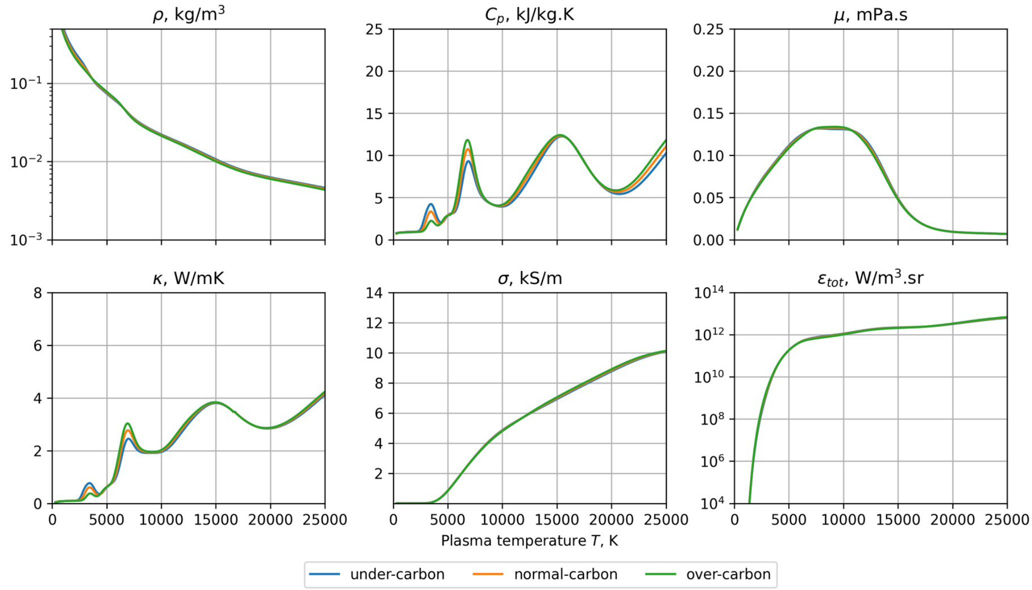

Figure 3—Plasma properties for gas compositions associated with FeCr slag at Ts = 1800 °C; clockwise from top left: density, heat capacity, viscosity, total radiation emission, electrical conductivity, and thermal conductivity

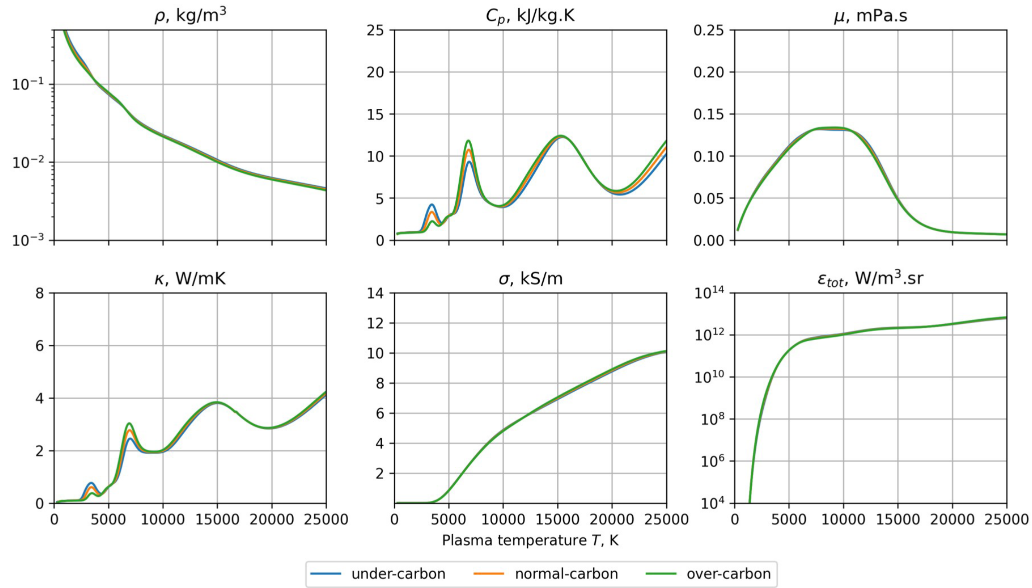

Figure 4—Plasma properties for gas compositions associated with FeCr slag at Ts = 3500 °C; clockwise from top left: density, heat capacity, viscosity, total radiation emission, electrical conductivity, and thermal conductivity

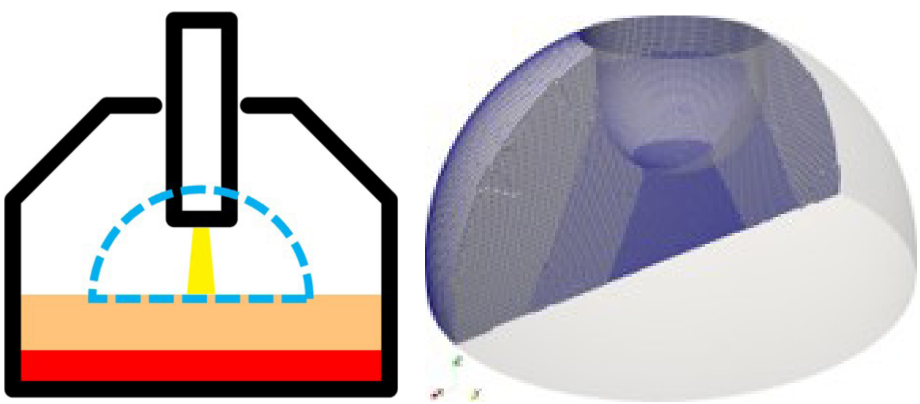

Figure 5—(l) schematic of DC furnace interior showing region modelled in blue outline, (r) rendering of model domain showing finite-volume mesh elements

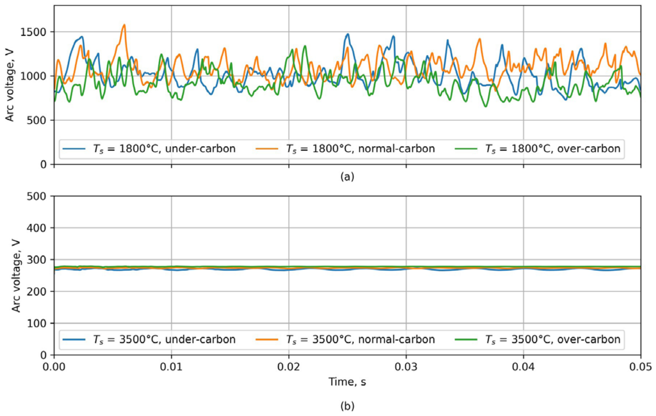

Figure 6—Arc voltages at 75 kA current and 0.4 m arc length, (a) slag temperature 1800 °C, (b) slag temperature 3500 °C

Effect of total radiation emission coefficient

In Figure 11 and Figure 12 the effect of changing the total radiation emission coefficient is shown. With all other properties kept the same the effect of increasing the carbon addition is to decrease the arc's conductivity, producing higher voltages. This is due to the increased reductant in the feed producing a freeboard gas, which generates a more emissive plasma, and although the interplay between absorption and emission can be complex in general three-dimensional arc structures, the nett effect in this particular case is that the arc column loses more energy by radiation as the emission coefficient increases. This cools the plasma and reduces the arc conductivity. As with the electrical conductivity, the effect is most marked for the under-carbon case, whereas the normal- and over-carbon cases are harder to distinguish statistically.

Comparing Figure 10 and Figure 12 with Figure 8 shows that the two plasma properties, which are most affected by the reductant balance at 1800 °C have an opposing effect; as carbon fraction

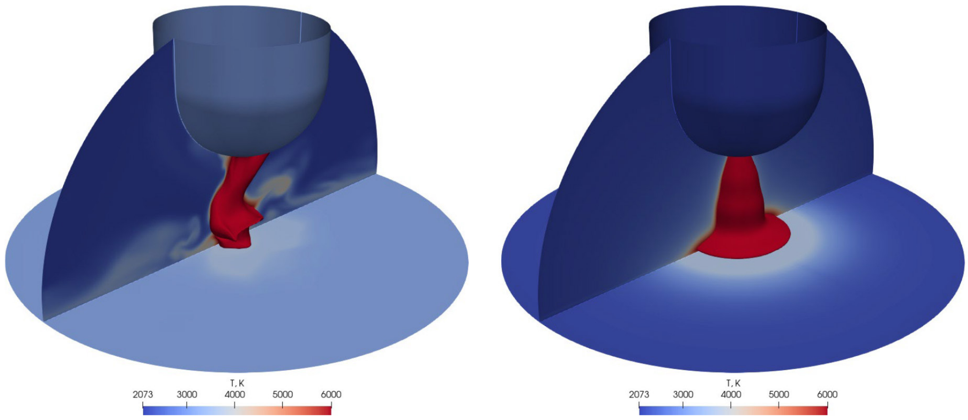

Figure 7—Visualisations of arc temperature field at 75 kA current, 0.4 m arc length, and normal-carbon balance, (l) slag temperature 1800 °C, (r) slag temperature 3500 °C

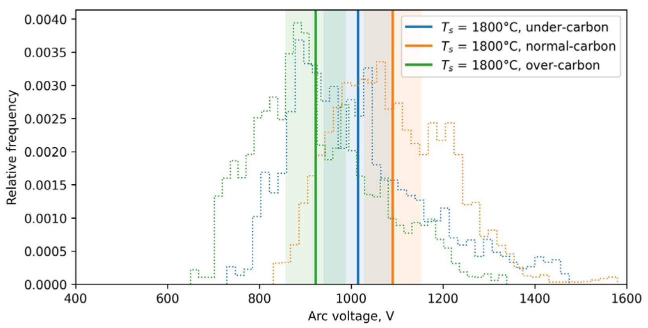

Figure 8—Statistical frequency plots of arc voltages at 75 kA current, 0.4 m arc length, and slag temperature 1800 °C (solid vertical lines are averages, and shaded areas are one standard deviation)

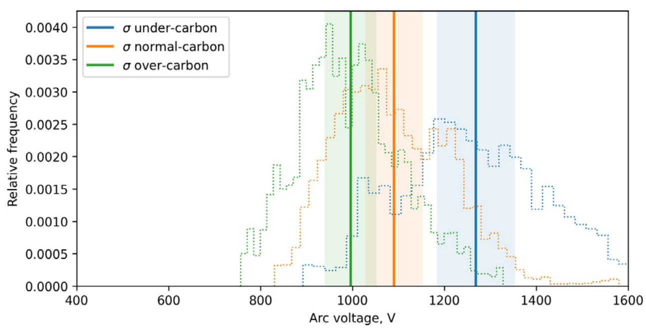

Figure 10—Statistical frequency plots of arc voltages showing the isolated effect of plasma electrical conductivity at slag temperature 1800 °C (solid vertical lines are averages, and shaded areas are one standard deviation)

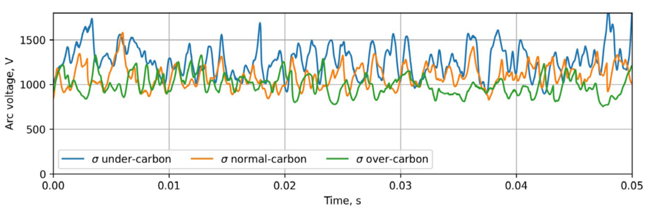

Figure 9—Arc voltages showing the isolated effect of plasma electrical conductivity at slag temperature 1800 °C

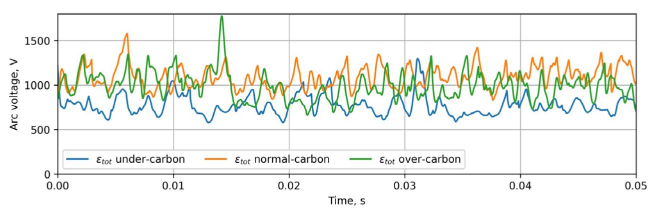

Figure 11—Arc voltages showing the isolated effect of radiation emission coefficient at slag temperature 1800 °C

increases, the electrical conductivity acts to make the arc less resistive as carbon fraction increases, while the emission coefficient acts to make it more resistive. For the particular set of conditions examined in the present work, it is interesting to note that the two effects are almost in balance and produce arcs with similar electrical properties.

Conclusions

A multi-stage computational modelling workflow was applied to the problem of plasma arc behaviour in DC furnaces for carbothermic FeCr production. In particular, the effect of changing the proportion of carbon reductant in the feed to the furnace was studied using a range of numerical calculation and simulation tools.

The equilibrium freeboard gas composition was significantly affected by the change in reductant balance, becoming progressively more contaminated with volatile species such as Mg and Si as the proportion of carbon was increased. This was, however, a second-order effect compared to increasing the effective slag temperature, which produced gases with much higher concentrations of metallic contaminants. Examining the thermophysical properties of plasmas arising from the different process gas compositions then showed that, at low slag temperatures the electrical conductivity and total radiation emission coefficient were most strongly affected, with both increasing as the reductant proportion in the feed was increased. At higher slag temperatures there was minimal effect of changing the reductant fraction, with only the peak values of thermal conductivity and heat capacity being affected over relatively small plasma temperature ranges. Finally, computational MHD simulations of arcs at scales comparable to industrial furnaces showed that changing the reductant balance in the feed had relatively little effect on the arc resistances and voltages produced. This was especially obvious at higher slag temperatures, where metal-contaminated arc plasmas all have similar properties. At lower slag temperatures, a basic sensitivity study showed that increasing electrical conductivity (associated with increasing reductant fraction) caused the arc to be less resistive, whereas increasing radiation emission coefficient (associated with increasing reductant fraction) caused more resistive arcs. Although both effects are quite strong in isolation, when acting together, they largely compensate for each other and produce arcs which display similar electrical behaviour.

It therefore seems unlikely that changes in feed reductant balance are the underlying cause of the large excursions in the electrode hoist position that are occasionally observed on operating DC furnace plants, at least in terms of the mechanism discussed

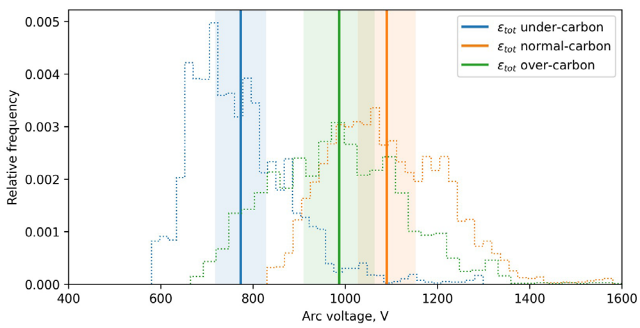

Figure 12—Statistical frequency plots of arc voltages showing the isolated effect of radiation emission coefficient at slag temperature 1800 °C (solid vertical lines are averages, and shaded areas are one standard deviation)

in the present work, whereby the reductant balance affects the freeboard gas composition and plasma properties. Future work in this area would be best directed toward studying the impact of feed contaminants such as moisture or organic volatiles, understanding the effective slag temperature and how to estimate appropriate values for it, and improving the performance of the computational models so that larger sets of data can be generated and analysed for improved statistical significance.

Acknowledgements

This paper is published with the permission of Mintek, and was supported by funding on Mintek Science Vote project IntelliMetTwin MCR-62604. The authors acknowledge the Centre for High Performance Computing (CHPC), South Africa, for providing computational resources for this research project.

References

Akhmetov, A., Zulhan, Z., Sadyk, Z., Burumbayev, A., Zhakan, A., Kabylkanov, S., Toleukadyr, R., Saulebek, Z., Ayaganova, Z., Makhambetov, Y. 2025. Carbon-Free Smelting of Ferrochrome Using FeAlSiCa Alloy. Processes vol. 13, pp. 1745. https://doi.org/10.3390/pr13061745

Bale, C.W., Bélisle, E., Chartrand, P., Decterov, S.A., Eriksson, G., Gheribi, A.E., Hack, K., Jung, I.-H., Kang, Y.-B., Melançon, J., Pelton, A.D., Petersen, S., Robelin, C., Sangster, J., Spencer, P., Van Ende, M.-A. 2016. *FactSage thermochemical software and databases*, 2010–2016. Calphad vol. 54, pp. 35–53. https://doi.org/10.1016/j.calphad.2016.05.002

Barcza, N.A., Curr, T.R., Jones, R.T. 1990. Metallurgy of open-bath plasma processes. *Pure and Applied Chemistry.* vol. 62, pp. 1761–1772. https://doi.org/10.1351/pac199062091761

Boulos, M.I., Fauchais, P.L., Pfender, E. 2023. Plasma in the Metallurgical Industry, in: Boulos, M.I., Fauchais, P.L., Pfender, E. (Eds.), Handbook of Thermal Plasmas. *Springer International Publishing*, Cham, pp. 1581–1660. https://doi.org/10.1007/978-3-030-84936-8_38

Bowman, B., Krüger, K. 2009. Arc Furnace Physics. Verlag Stahleisen GmbH, Düsseldorf, Germany.

Dalaker, H., Hovig, E.W. 2023. Hydrogen Plasma-Based Reduction of Metal Oxides, in: Fleuriault, C., Steenkamp, J.D., Gregurek, D., White, J.F., Reynolds, Q.G., Mackey, P.J., Hockaday, S.A.C. (Eds.), Advances in Pyrometallurgy, *The Minerals, Metals & Materials Series*. Springer Nature Switzerland, Cham, pp. 85–94. https://doi.org/10.1007/978-3-031-22634-2_8

Gasik, M. (Ed.). 2013. Handbook of ferroalloys: Theory and Technology. Elsevier/Butterworth-Heinemann, Amsterdam.

Geldenhuys, I.J. 2013. Aspects of DC chromite smelting at Mintek - an overview, in: Efficient Technologies in Ferroalloy Industry: Proceedings of the Thirteenth International Ferroalloys Congress, International Ferroalloys Congress. Presented at the 13th International Ferroalloys Congress, *Public Association INFACON XIII,* Almaty, Kazakhstan, pp. 31–47.

Geldenhuys, I.J. 2017. The Exact Art and Subtle Science of DC Smelting: Practical Perspectives on the Hot Zone. JOM 69, pp. 343–350. https://doi.org/10.1007/s11837-016-2171-z

Jones, R.T. 2014. DC arc furnaces – past, present, and future, in: Celebrating the Megascale: Proceedings of the Extraction and

Processing Division Symposium on Pyrometallurgy in Honor of David G.C. Robertson. Presented at the TMS Annual Meeting 2014, *TMS (The Minerals, Metals & Materials Society)*, pp. 129–139.

Kjellberg, B., Stenkvist, S.E. 1989. DC Technology for Smelting Furnaces, in: INFACON '89: The 5th International Ferroalloys Congress. Presented at the 5th International Ferroalloys Congress (INFACON V), *The Ferroalloys Association*, New Orleans, USA, pp. 88–94.

OpenCFD Ltd. 2025. OpenFOAM v2506, https://www.openfoam.com/ [WWW Document]. URL https://www.openfoam.com/ (accessed 8.17.25).

Oterdoom, H., Reuter, M., Zietsman, J. 2025. DC Ferrochrome Smelting: The Arcing Zone and Its Influence on Energy Transport and Exergy Dissipation. *Metallurgical and Materials Transactions B* vol. 56, pp. 890–912. https://doi.org/10.1007/s11663-024-03365-y

Reynolds, Q.G. 2020. Toward computational models of arc dynamics in silicon smelters, in: 14th International Conference on CFD in the Oil & Gas, Metallurgical and Process Industries. *Presented at the 14th International Conference on CFD in the Oil & Gas, Metallurgical and Process Industries, SINTEF Academic Press*, Trondheim, Norway, pp. 99–106.

Reynolds, Q.G., Bowman, B., Erwee, M.W., Geldenhuys, I.J., Sandrock, C., Venter, G.A., Xakalashe, B.S., Zietsman, J. 2025a. Plasma soup for the pyrometallurgist's soul. J. *South African Institute of Mining and Metallurgy*. vol. 125, pp. 129–144. https://doi.org/10.17159/2411-9717/758/2025

Reynolds, Q.G., Sandrock, C., Goutier, P.-A., 2025b. minplascalc, https://github.com/quinnreynolds/minplascalc/releases/tag/v1.0.2.

Reynolds, Q.G. 2026. plasmaArc, https://github.com/quinnreynolds/plasmaArc/releases/tag/v1.1.1-openfoam-v2512.

Reynolds, Q.G., Xakalashe, B.S., Tsebe, S.P., Erwee, M.W., Jones, R.T., Geldenhuys, I.J. 2026. Plasma arc behaviour in DC arc furnace smelting of PGM-bearing materials: a modelling study on the effect of reductant choice. J. *South African Institute of Mining and Metallurgy*. Article in press.

Sager, D., Grant, D., Stadler, R., Schreiter, T. 2010. Low cost ferroalloy extraction in DC-arc furnace at Middelburg Ferrochrome, in: Proceedings of the Twelfth International Ferroalloys Congress - Sustainable Future. *Presented at the 12th International Ferroalloys Congress (INFACON XII)*, Outotec Oyj, Helsinki, Finland, pp. 803–814.

Sommerfeld, M., Botinha, R., Friedrich, B. 2024. Enabling CO2 neutral metallurgy for ferrochromium production using bio-based reducing agents. Scientific Reports. vol. 14, pp. 10878. https://doi.org/10.1038/s41598-024-61700-4

Swanepoel, S., Garbers-Craig, A.M., De Villiers, J.P.R. 2022. The Oxidation Behavior of a Selection of South African Chromites. Metallurgical and Materials Transactions B vol. 53, pp. 3805–3824. https://doi.org/10.1007/s11663-022-02643-x ◆